PNNL-SA-26121

Pacific Northwest
NATIONAL LABORATORY

Proudly Operated by Battelle *Since 1965*

Preliminary Test Methodology for Linear Reciprocating Ball-on-Flat In situ Friction and Wear Studies of Polymers in High Pressure Hydrogen

December 2016

Alvine
Duranty
Pitman
Roosendaal
Brooks
Simmons

U.S. DEPARTMENT OF ENERGY

Prepared for the U.S. Department of Energy
under Contract DE-AC05-76RL01830

PNNL-SA-26121

Preliminary Test Methodology for Linear Reciprocating Ball-on-Flat In situ Friction and Wear Studies of Polymers in High Pressure Hydrogen

Alvine
Duranty
Pitman
Roosendaal
Brooks
Simmons

December 2016

Prepared for
the U.S. Department of Energy
under Contract DE-AC05-76RL01830

Pacific Northwest National Laboratory
Richland, Washington 99352

Abstract

This test methodology describes in situ testing of friction and wear (tribology) of polymers under high pressure hydrogen. This methodology is based in part on the existing tribological standard ASTM G133 "standard test method for linearly reciprocating ball-on-flat sliding wear". Friction and wear testing under a high-pressure hydrogen environment is critical for hydrogen fueling infrastructure components such as compressors, valves and other actuated devices. Here we present test a methodology for in situ friction and wear studies of polymers under 28 MPa (4,000 psi) hydrogen in a linear reciprocating custom built apparatus. Supporting data from in situ acrylonitrile-butadiene rubber (NBR, commercially Buna-N) tests in 28 MPa (4,000 psi) hydrogen are presented.

Contents

Figures

Tables

1.0 Disclaimers

Disclaimer 1: While this test methodology is based in part on an existing ASTM standard (G133), and presented in a format similar to the ASTM format, the Pacific Northwest National Laboratory is not in any way affiliated with ASTM, nor has this test methodology been sanctioned or approved in any way by ASTM.

Disclaimer 2: Before using the information presented in this test methodology, you must first evaluate the methodology and determine if it is suitable for your intended application. You assume all risks and liability associated with such use. Pacific Northwest National Laboratory makes NO WARRANTIES, including, but not limited to, any implied warranty or warranty of fitness for a particular purpose. Pacific Northwest National Laboratory will not be held liable for any loss or damage arising from the use of the information presented herein, whether direct, indirect, special, incidental, or consequential.

Warning: Gaseous hydrogen is odorless, colorless and tasteless and thus undetectable by human senses. Hydrogen is highly flammable and burns with a nearly invisible blue flame and can form explosive mixtures in the presence of oxygen. High pressures in excess of 7 MPa (1,000 psi) add additional explosion hazards that must be planned for in preparation for any testing. Pacific Northwest National Laboratory will not be held liable for any loss or damage arising from the use of the information presented herein, whether direct, indirect, special, incidental, or consequential.

2.0 Motivation and Background

Hydrogen is under consideration as an alternative for use in zero-emission vehicles (ZEV).[1, 2] However, as with any other new technology, hydrogen power presents multiple materials science challenges for infrastructure applications.[2-4] Of primary concern is materials degradation in high pressure hydrogen environments[1-61]. There is special concern for components exposed for long periods of time or exposed to cyclic pressures or temperatures. This is known to be especially problematic for certain metals that when exposed to hydrogen degrade by forming hydrides and swelling, undergoing surface blistering, or material embrittlement.[2, 23, 53, 62, 63] Non-metallics are not immune to hydrogen compatibility effects. Piezoelectric ceramic materials, such as lead zirconate titanate (PZT), used in high-pressure hydrogen actuators undergo degradation under high-pressure hydrogen in the form of blistering or lead (Pb) migration.[8, 19, 28, 64] Elastomers used in O-rings and thermoplastics used in compressor valves and seals may also see significant high-pressure hydrogen exposure in hydrogen infrastructure applications.[3, 34, 65] Other examples include structural polymers such as high-density polyethylene (HDPE) and nylon which are used as liners in high-pressure pipelines[43] and type IV hydrogen tanks[42, 49, 66] and Delrin used in hoses.

While there is an abundance of research into hydrogen effects on metals and even piezoelectrics, there is comparatively little information in the literature about the potentially damaging effects of hydrogen on polymers.[3-5, 11, 12, 16, 18, 27, 43, 56, 59-61, 65, 67-74] There have been some limited investigations on tensile properties of high-density polyethylene (HDPE)[5] and the tribological properties of neat semi-crystalline polytetrafluoroethylene (PTFE)[12, 72, 73] and PTFE composites[68-71] in high pressure hydrogen. However, additional studies are needed to fully understand the effects of hydrogen over a broader range of materials and pressures. In particular, tribological studies with elastomers are lacking. The process of hydrogen absorption in polymers is different from absorption in metals[62] due to a lack of disassociation in the polymer. As a result, the majority of effects are expected to be mechanical rather than chemical in nature as with metals or piezoelectrics. Damaging effects may include bubble or void formation, surface

blistering, dilation, changes in modulus and strength, and other changes associated with the absorption of a relatively high amount of hydrogen.[5] Additionally, since the saturation hydrogen concentration in polymers is proportional to the exterior pressure it is thus expected that the damaging effects are more serious at higher pressures.[42, 49, 66]

3.0 Scope

This test method covers laboratory procedures for determining the in situ coefficient of friction and wear rates in a high-pressure hydrogen environment of polymeric materials using a ball-on-flat reciprocating geometry similar to ASTM G133. This method should also be applicable for ceramics and metals with some modifications to account for ball wear, and for non-linear tests, but it has not been validated for these material classes or tests yet. Supporting data from in situ NBR tests in 28 MPa (4,000 psi) hydrogen are presented.

4.0 References and Standards

ASTM G133 – Standard Test Method for Linearly Reciprocating Ball-on-Flat Sliding Wear

ISO 6601 – Plastics – Friction and Wear by Sliding – Identification of Test Parameters

SAE J2579 – Standard for Fuel Systems in Fuel Cell and other Hydrogen Vehicles

SAE J2601 – Fueling Protocols for Light Duty Gaseous Hydrogen Service Vehicles

GTR – Global Technical Regulation

ISO 11114-2 – Gas cylinders – compatibility of cylinder and valve materials with gas contents – Part 2: Non-metallic materials

SAND2012-7321 - Sandia Technical Reference for Hydrogen Compatibility of Materials: Section 8100

CSA/ANSI CHMC 1-2014 – Test Methods for Evaluating Material Compatibility in Compressed Hydrogen Applications – Metals

5.0 New Terminology

Swelling – either in situ or ex situ expansion of the test material due to absorption of the test gas. This may be due to chemical reactions (hydride formation) of fillers within the material, or due to unbalanced forces from absorbed gases during or after decompression.

Saturation time – the point at which the test material will no longer absorb additional gas. This is determined by the diffusion rate and saturation concentration of the particular gas in the material at a given temperature and pressure.

Explosive Decompression – refers to rapid release of the gas pressure from the test vessel relative to the diffusion rate of the gas in the material. This can lead to surface blistering and other damage.

Blistering – damage to the surface of a test sample in the form of localized bubbles that can be intact or ruptured and typically caused by unbalanced pressure of trapped gas within the sample during rapid decompression.

Viscoelasticity – describes the time dependent response of polymers to local deformation through a combination of viscous flow and elastic response.

Hardness – is the resistance of the polymer to localized deformation. Since polymers can be viscoelastic, this property can be time dependent.

Adhesive wear – describes the transfer of material from one surface to the other due to direct contact and plastic deformation. The applied load breaks bonds and can permanently transfer materials from one surface to the other.[75]

Abrasive wear – describes the wear of the softer material due to hard protuberances or particles on the harder surface. This can occur as cutting which results in material loss or ploughing in which material is pushed out of the wear track and not removed from the surface. [75]

Transfer Film – in adhesive wear between a hard and soft material, a film of the softer material can build up on the harder surface. Typically, this is the buildup of a thin polymer film on a metal surface. The presence of this film can then modify the friction and subsequent wear behavior.

Stick-slip – described as a situation where the surfaces moving across each other alternate between sticking and sliding. This can result in oscillations in the coefficient of friction.

6.0 Summary of Test Method

This test method describes the in situ measurement of friction and wear of polymer samples under a high pressure hydrogen environment. The system is configured for linear reciprocating motion of a steel ball across the polymer sample in a sliding or rubbing motion under established parameters. During the motion, a normal load is applied to the stationary metal ball by a series of weights. Frictional force and wear depth are measured in situ as the test progresses.

The following parameters can be varied for each test: velocity, normal load, and wear track length. The system is set up to rapidly accelerate at the turn around points of the wear track.

For the tests, the entire test apparatus is placed in a high pressure autoclave and pressurized to the desired pressure with the test gas of choice. The particular system used for these tests can only be charged to a maximum 34 MPa (5,000 psi) with high purity hydrogen or inert gas, but the in situ tribometer apparatus should be usable to much higher pressures such as 103-138 MPa (15-20,000 psi). Electrical feedthroughs in the autoclave lid provide power and electrical connections for the electronics package. The device is computer controlled via a system located external to the autoclave.

7.0 Significance and Use

This test is designed to mimic dynamic sliding friction under a high pressure hydrogen environment as might be experienced by a polymeric sliding seal in a compressor piston or mechanical valve with an o-ring seal. While the pressures reported here are only 28 MPa (4,000 psi), the test methodology should be applicable to pressures as high as 103-138 MPa (15-20,000 psi), as long as care is taken for potential swelling of the polymers with regards to sample mounting. Lower pressure measurements and comparison inert gas tests are also applicable.

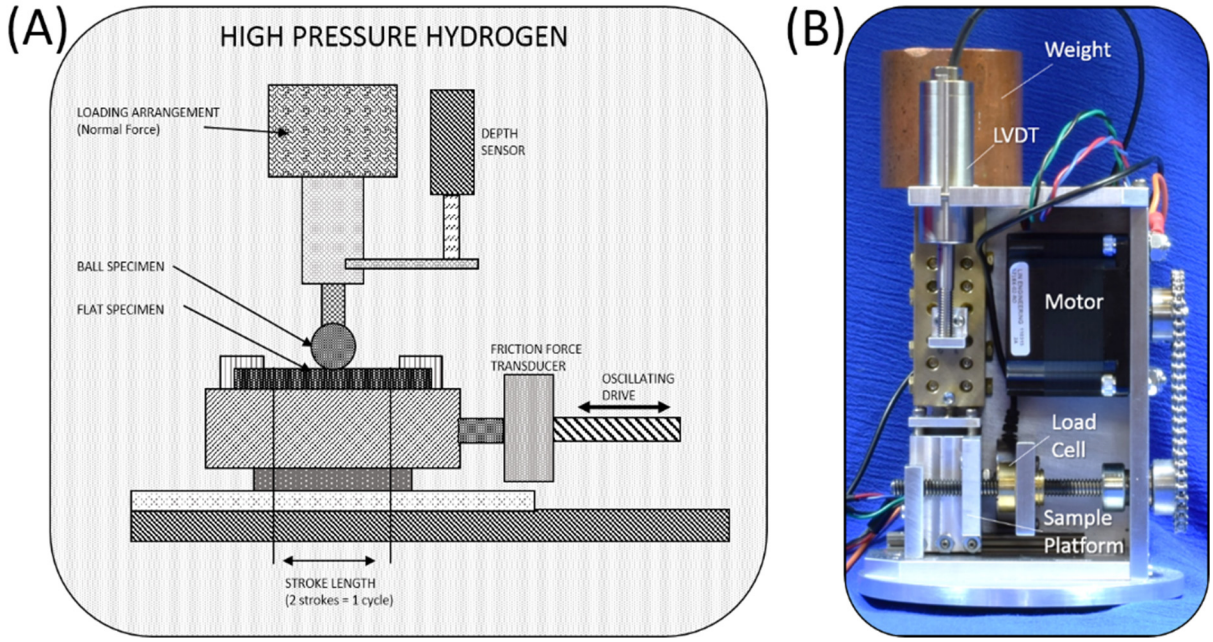

Figure 1. (A) Schematic of the in situ tribometer to measure friction and wear in a high pressure hydrogen environment.

8.0 Test Gap Identification

This methodology should be considered preliminary as it is lacking the following additional tests which are planned in future years of research.

1. Full mapping of the dependence of velocity, and loading. These tests are important as the combination of velocity and loading influence both the heating and local deformation of the polymer. Polymer wear is known to be highly dependent on velocity and loading.[75]

2. Full mapping of wear time. Since the friction and wear are dependent on the development of a transfer layer and heating of the sample, it is important to measure the friction and wear at multiple different numbers of cycling to look for trends. This will be dependent on loading, velocity, environment, and material.

3. Testing of multiple thermoplastics and elastomers. There is considerable variation between similar polymers and even what is nominally the same polymer from different vendors. This is

influenced by processing conditions, additives, cross-linking, and thermal history. It is important to look at same species and cross-species variation to achieve a full understanding of the impacts of hydrogen on polymer friction and wear.

4. Complete cross-referenced calibration standards across multiple environments. A good calibration standard is important to cross check between different systems. An ideal case would be to use a minimum of three different materials with coefficients of friction and wear behavior that span most polymers.

5. Complete environmental cross comparison as a function of gases (hydrogen, helium, argon, nitrogen), and humidity. This is important to establish the roles of humidity, pressure, and gas species on friction and wear.

6. Thermally controlled measurements between -40 and +85 °C to fully simulate the hydrogen refueling environment. Polymers in a hydrogen infrastructure role may experience temperatures in this range. Temperatures strongly influence polymer mechanical behavior, expansion, and wear.[75]

7. Full mapping of the effect of hydrogen pressure from ambient to 34 MPa (5,000 psi) and higher pressures up to 103 MPa (15,000 psi). While it is unlikely there are many abrupt transitions as a function of temperature, the solubility of hydrogen is expected to increase proportionally with increasing pressure. This means that effects will likely become more prominent with increasing pressure.

8. Effects of pressure cycling. Pressure cycling is likely to be present for most, if not all hydrogen infrastructure applications of polymers. Further, rapid pressurization may induce compression damage through plastic deformation and may also induce damage through explosive decompression and the subsequent formation of surface or subsurface blistering or damage. This damage is likely to strongly influence friction and wear behavior.

9. Comparison tests on sample thickness. The pin will locally compress and deform the polymer as it moves. Dependent on the thickness, this deformation can potentially be influenced by the lower sample mounting plate. We are trying to mitigate this effect by making the sample thickness at least one ball radius thick, but empirical testing should be completed to investigate this effect as it would be an issue in real world applications.

10. Lateral compression may play a role. As with thickness, the potential lateral compression of the sample as would be the case with an o-ring may be of importance. Shear stresses may play a role. More experimentation and a sensitivity analysis needs to be done on sample mounting to ensure that potential impacts from this are fully understood.

9.0 Apparatus

9.1 General Design and Use

Figure 1A shows the general schematic of the in situ tribometer and Figure 1B shows the actual device outside of the high pressure hydrogen autoclave. Figure 2 shows the pin and sample geometry in greater detail. The system works by pressing a ball (See Figure 2A, B) normally into the sample which moves in a linear reciprocating fashion. The loading on the ball is applied through a series of dead weights set on top of the ball carriage system which is free to move in the vertical direction while a computer controlled stepper motor drive provides the horizontal linear motion of the sample stage. The motor drive is coupled

to the sample stage by means of a capacitive load cell which measures the horizontal force on the stage induced by the friction of the ball on the sample. Wear depth of the ball into the sample is measured in the vertical direction by means of a linear position sensor mounted on the ball carriage. Custom software controls the stepper motor and subsequently the linear reciprocating motion of the sample stage to achieve nearly constant velocity over 95% of the travel in both directions.

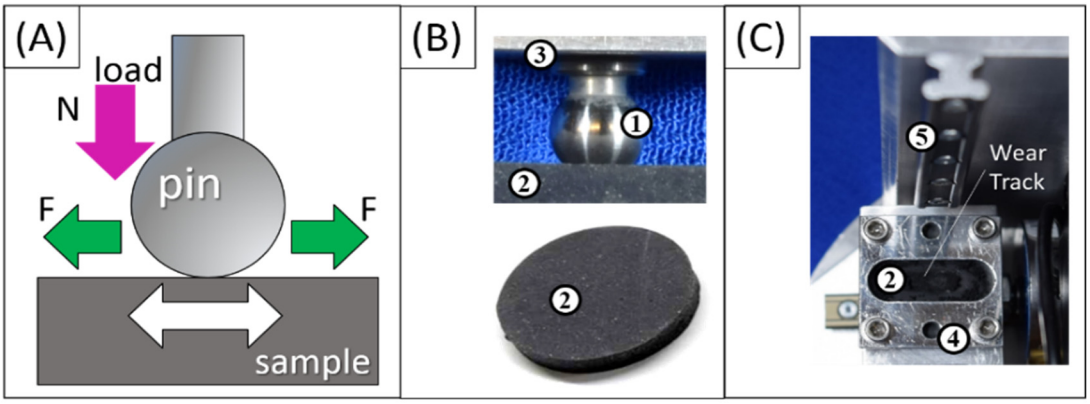

Figure 2. (A) Schematic of sample moving against the static steel ball where *N* is the normal force exerted by the load and *F* is the frictional load. (B) Photograph of the static steel ball (1) held by the holder (3) and elastomeric sample. (C) Image of the key-hole mount (4) that secures the sample (2) and the high-precision rail on which the ball-holder moves (5).

After sample loading, the entire apparatus is lowered into the high pressure hydrogen autoclave and sealed, where the design of the system ensures that the apparatus is level inside the sealed autoclave. Sealing is accomplished by a Teflon wrapped steel lens ring between the vessel and the vessel lid. Electrical contact and power to the apparatus is provided by means of electrical feedthroughs into the system. The system is then flushed with high purity argon gas to displace atmospheric O_2 present down to < 1ppm levels. The argon is then flushed with low (<3 MPa, 500 psi) gas of choice (hydrogen or argon) and then pressurized to the set pressure (up to 34 MPa, 5,000 psi) over a 15 minute period at approximately 2 MPa/min (300 psi/min). The system is then left to equilibrate for a 12 hour period to ensure gas saturation in the sample, temperature equilibrium, and to settle mechanically.

Tests are run under the following conditions: 1) high pressure hydrogen up to 34 MPa (5,000 psi), 2) high pressure argon, 3) ambient air conditions. These different environments allow for cross-comparisons to identify which environmental factors are most impactful. Such factors include influence of gas species, pressure, and humidity. As noted above, additional testing is required, for a complete understanding.

9.2 Critical Design Features

There are several critical design features to address for high pressure hydrogen testing, the first is materials compatibility. One must avoid use of materials or components that are known to be affected by hydrogen or by high pressure. This means avoiding components with seals that can be crushed or that can trap diffused gas. Additionally, one must avoid materials capable of hydriding in the presence of hydrogen gas such as neodymium (Nd). For example, one should avoid Nd based motors even though the power ratings are much higher than for ferrous-based motors. The Nd magnets in the motors are known to hydride and swell, rendering the motor unusable in short order in a high-pressure hydrogen environment. For safety reasons, one should also avoid known spark sources such as brushed motors. Additionally, one should avoid materials that may off-gas large amounts of oxygen.

9.3 Critical Testing Criteria

There are multiple factors that may influence differences in friction and wear for samples in high pressure hydrogen as compared to ambient air or other environments. These are: 1) pressure, 2) humidity, and 3) gas species. Each of these factors may influence the friction and wear factor in hydrogen as compared to ambient air results. To this end, it is important to carry out enough tests so that one can distinguish the different factors. This means that one must complete comparison tests between high-pressure hydrogen and an inert gas like argon at the same pressures, as well as tests of different humidity. Humidity is known to strongly impact tribology in some elastomers and hydrogen systems are typically extremely dry systems.

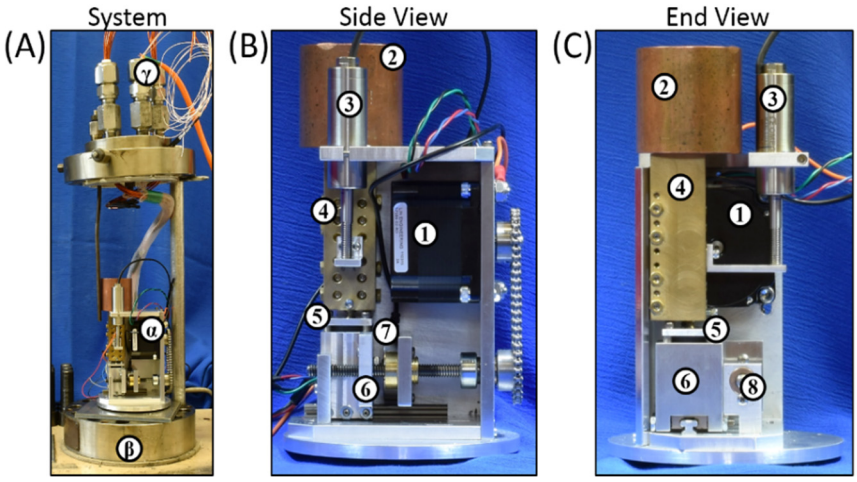

Figure 3. (A) System image containing tribometer and autoclave. (B) Side view of the tribometer instrument. (C) End view of the tribometer.

9.4 Specifics of the Apparatus

Figure 3A shows the apparatus and the high-pressure autoclave. The in situ tester (α) fits within the high-pressure vessel (β), and is controlled remotely through electrical feed-throughs (γ). The in situ device is shown in close-up from two different viewpoints in Figure 3B and C. The functional parts of the apparatus are as follows. The side view of the tribometer contained in Figure 3B shows the stepper motor (B.1) attached to a drive chain that moves the sample stage (B.6) and secured sample (B.5), the copper dead weight that exerts a normal force on the sample (B.2), and the static ball holder (B.4). The capacitive load cell (B.7) coupled with the sample sled collects the frictional load data while a linear variable differential transformer (LVDT) (B.3) is attached to the static ball holder that collects real-time measurements on the relative depth of the ball into the polymer surface. The sample stage and static ball holder both move on lubricated high precision rails to minimize hitching that might contribute to the measured frictional load. These rails can be seen in Figure 2C and also in Figure 2C which also contains an end view of the lead screw that drives the sample sled and the hard stop preventing the sample sled from leaving the lead screw (2C.8).

9.5 Calibration

Calibration is critical to achieving meaningful and reproducible results. For these tests, a calibration must be run for each gas at each pressure of interest. Both the load cell and the LVDT require calibration.

Load cell: The load cell used in this system is a miniature capacitive load cell that is unsealed to the local environment. It is critical that the cell is unsealed as the pressures reached in these tests could potentially crush a seal or if gas were to diffuse into it, cause it to rupture upon depressurization. Due to the

capacitive nature of the load cell, the measured load is related to the permittivity of the gas at pressure and the separation of the plates of the capacitor. Thus, one should expect that the load calibration is dependent on both the gas species and on the pressure.

LVDT: The vertical position sensor is a miniature linear voltage differential transformer (LVDT) which is similar in design to a solenoid where small changes in the displacement of the center pole results in changes in voltage which are converted to measured displacement. We are using an unsealed design compatible for use in high pressures.

The LVDT and load cell are calibrated simultaneously at a given pressure and gas species by using a wedge-shaped steel sample and a rolling ball as seen in Figure 4 rather than the static ball used for testing. Only the load in the pin holder is used in the calibration with no additional weights. A rolling ball is used to minimize wear of the calibration wedge. As the ball rolls in a reciprocating fashion over the wedge it measures the profile of the wedge such as in

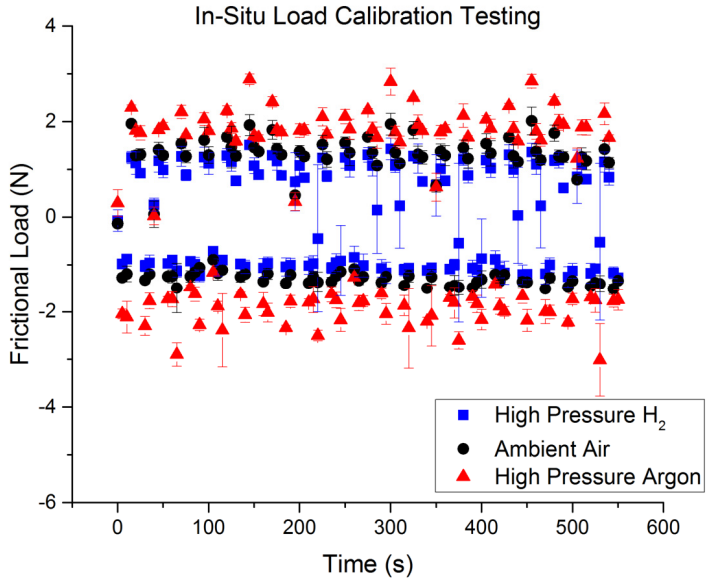

Figure 6, which can then be compared to measurements at ambient conditions to calibrate the LVDT. Simultaneously the frictional drag on the sled is measured with the load cell and can also be calibrated by comparison to the identical test at ambient conditions as in Figure 5. In this manner, the calibration can be used at each pressure and for each gas species to ensure that influences on the measurement are accounted for.

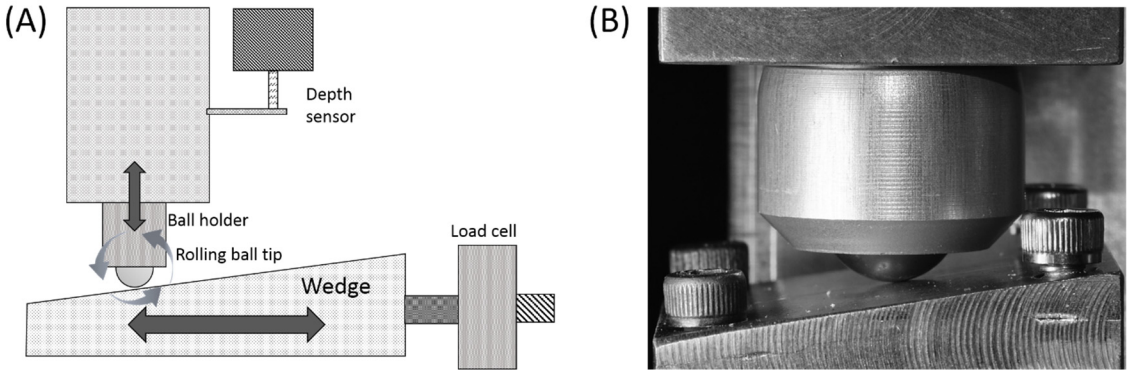

Figure 4. (A) Schematic of the setup for calibration of the tribometer load cell and LVDT. (B) Image of calibration rolling ball on wedge.

Two assumptions that were made for these calibration tests are that for rolling friction of steel on steel at relatively low velocity and on smooth surfaces that the frictional force should not be dependent on the environment that the tester is exposed to. Likewise, since the number of cycles used for calibration are low (< 20) and the speed relatively low, there should be minimal wear. Thus, the change in height of the ball should also not be dependent on the environment. Based on these reasonable assumptions we can then use these identical measurement sets to extract the proportional multiplier for the load cell as a function of gas species and pressure, as well as for any corrections to the LVDT. Potential deviations from the ideal behavior expected from our assumptions may include velocity, pressure, and gas species dependence to displace gas as the sample sled moves back and forth. This would present as "air" resistance or drag and should be proportional to the velocity and to the gas density. Since argon has approximately 20 times the density of hydrogen, this effect will be more noticeable in argon and may account for the spikes in the load at the turn around points of the sled. Further testing as a function of velocity is needed to determine at what point this becomes an issue (if at all).

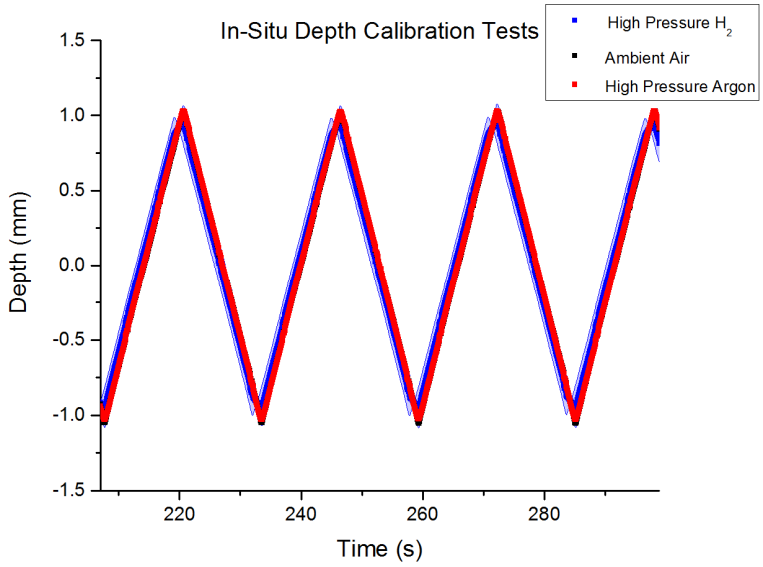

Figure 5. Calibration data for different environments. In experiments to date, the differences have been less than 2.5% which is within the uncertainty of the position data.

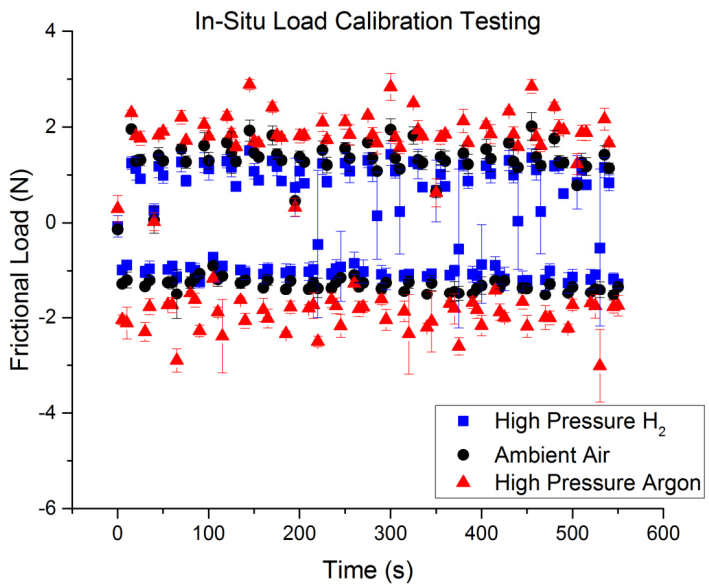

Figure 6. Calibration data for the load cell for different environments. The mean of the data is then used to extract the linear normalization parameter by comparison with the air data for correction.

10.0 Procedure

10.1 Sample Preparation Guidelines

Samples ideally should be cut or machined from sheet or gasket material at least 1/8th inch in thickness. This makes the samples at least one full radius of the static ball in thickness and typically at least five times the maximum penetration depth of the ball. This minimum thickness was chosen to mitigate potential thickness dependent results. The backing plate upon which the sample rests should be smooth and free of any holes or ridges that could impact the measurement.

Prior to sample use, the samples should be washed with detergent and water to remove any residual oils or talc. The presence of these surface treatments can significantly impact the test by increasing scatter in the data at short times. Samples should then be dried at elevated temperatures appropriate to the working temperature of the material, taking care not to exceed approximately 85% of the working temperature to not damage the material. This drives off excess water that may have accumulated during washing for hydroscopic samples. After drying, the samples should then be stored in a controlled humidity environment prior to actual testing. This protocol should be evaluated for different materials in regards to their interaction with water and thermal stability.

It is also critical to ensure that for all comparison tests that the samples are all from the same vendor batch, since batch to batch variations may significantly influence the testing results. Additionally, samples should all be prepared with the same orientation to reduce the influence of surface variations resulting from processing on testing. This is likely more important in semicrystalline material, but the same protocol should still be adopted for all materials as there may be directional effects from additives as well.

Samples are loaded into a custom made key-hole mounting bracket shown as B.5 and C.5 in Figure 3 with a smooth lower plate. The top key-hole plate offers a large surface area to grip the sample with an opening for the ball to move freely on the surface of the sample. Previous trials were attempted with only corner mounting of the sample but proved ineffective to hold the sample flat and led to significantly more variation

in sample-to-sample results. Using this mounting method, sample-to-sample variation was approximately 7% under ambient conditions in both the in situ tester and with a linear reciprocating commercial tester.

10.2 Testing in Ambient Air

Experiments are performed in ambient air conditions to provide a basis of comparison for measurements performed in high pressure hydrogen and high pressure argon. This is meant to mimic standard tests that may be done on samples for wear. Tests are also performed with the in situ tester inside the autoclave to closely represent the same conditions experienced during the high pressure runs. Representative temperature and relative humidity measurements of the ambient environment inside the autoclave range from 21-24 °C and 35 - 46% respectively. Once the tribometer is prepared, the stepper motor is run for 120 linear reciprocating cycles of the sample sled which takes approximately 60 minutes during which frictional load data is recorded. After the wear tests are complete, the samples are unloaded and then the wear track is imaged using a Keyence VHX-1000 microscope to qualitatively assess wear damage and measure track depth. This ex situ post mortem is carried out for all pressures and gas species.

10.3 Testing in High Pressure Hydrogen

The in situ hydrogen experiments are performed at 28 MPa (4,000 psi) inside a 15.5 L autoclave pictured in Fig. 2A. The tribometer is prepared for the experiments by mounting the samples and dead weights in the same manner as the ambient air tests. Once power and data electrical connections are made, the tribometer is lowered into the autoclave. The cylindrical form factor and size of the in situ tester ensures proper vertical alignment of the load column to within 2 degrees. The autoclave cover containing all the electrical feedthroughs is then lowered onto a lens ring wrapped in Teflon tape and bolted onto the autoclave body. The bolts are torqued to 285 Nm to ensure a proper seal and prevent hydrogen leakage. 0.5 MPa (80 psi) argon is then flowed through the autoclave to displace any oxygen that may still be present. Once argon has flowed for approximately one hour, the autoclave is then pressurized with hydrogen containing 0.5 ppm O_2 and H_2O in roughly 1.4 MPa (200 psi) steps to a final pressure of 28 MPa (4,000 psi). During the pressurization process an O_2 sensor is used to monitor the amount of O_2 present in the hydrogen flowing into the autoclave. The sample is soaked in hydrogen for eight hours to ensure complete saturation of the sample. Based on calculations using the literature values of the hydrogen diffusion rate in NBR, this should occur after approximately 2 hours for a sample thickness of 22 mm. The high-pressure hydrogen experiment is then carried out in the same fashion as the ambient air experiments. After the experiment is complete, the autoclave is slowly depressurized at approximately 0.34 MPa/s (50 psi/s) and the tribometer is then removed. The samples are then unloaded and analyzed for wear damage.

10.4 Testing in High Pressure Argon

The in situ argon experiments are performed at 24 MPa (3,500 psi) under nearly identical conditions to the high-pressure hydrogen tests. The slightly lower pressure is used due to much larger increase in temperature upon initial pressurization and subsequent drop in pressure upon cooling to room temperature. As in hydrogen testing, 0.55 MPa (80 psi) argon is then flowed through the autoclave to displace any oxygen that may still be present and confirmed to levels less than 10 ppm after approximately one hour. Once the required oxygen levels have been reached, the autoclave is then pressurized with high pressure argon containing 0.5 ppm O_2 and H_2O in roughly 7 MPa (1,000 psi) steps to a final pressure of 28 MPa (4,000 psi). After cooling, the pressure drops to about 24 MPa (3,500 psi). The sample is soaked in the argon for at least 12 hours to ensure complete saturation of the sample with argon. After the experiment is complete, the autoclave is slowly depressurized at approximately 0.34 MPa/s (50 psi/s) and the tribometer is then removed. The samples are then unloaded and analyzed for wear damage.

11.0 Measurement and Analysis

The frictional force between the sample and the ball during the linear reciprocating motion is measured by the horizontal load cell and represents the force required to move the sample at the constant prescribed velocity. This frictional force, F, is related to the normal force, F_N, exerted by the ball and the set loading, by the coefficient of friction, μ, via the relationship in Eq. (1).[75] Figure 7 shows representative frictional load data for a single cycle consisting of a forward motion of the sample sled where F is arbitrarily denoted as negative and the reverse motion where F is denoted positive. Note that the load cell is tared or set to zero before each measurement set to discard any offset which does not provide meaningful information in this test. All analysis will be based on peak to peak amplitude of the load. Due to the nature of the linear-reciprocating mode, the peaks in F at the beginning of each motion of the sample sled measurements of the static friction load, F_s, or the force required to move the sample sled from a complete stop. The plateau regions immediately after the F_s peaks contain information about F_k, the coefficient of kinetic (or dynamic) friction, which describes the frictional force between two moving surfaces.

$$\mu = \frac{F}{F_N}$$

Equation 1. Relationship between the frictional force F, normal force FN and the coefficient of friction μ.

As noted above, at this point we are basing the analysis only on a peak to peak analysis of the static friction. At a later date, we will refine the analysis to separate the effects on both the static and dynamic coefficients of friction. However, for the elastomers tested to date, the difference between the two appears to be a secondary effect. This is not expected to be the case for some thermoplastics like PTFE where the dynamic friction can be higher than the static friction.

Direct comparison of the load cell data between high-pressure hydrogen and ambient air illustrates some important aspects. The results of several ambient and high pressure (28 MPa, 4,000 psi) experiments are shown in Figure 8 which also compare the coefficient of static friction for NBR samples. In Fig. 8A, the characteristic frictional load curves for a single cycle in ambient air (black data) is overlaid with the frictional load curve obtained in hydrogen (blue data). In these data, the amplitude of the cycle in hydrogen is 29.8% greater than the amplitude of the ambient air cycle.

This increase in frictional load indicates that more force is required to slide the ball across the sample in high pressure hydrogen than in air. The data presented in Fig. 8B show the coefficients of static friction for a series of ambient air tests (black data) and 28 MPa (4,000 psi) high pressure hydrogen tests (blue data) that were calculated by halving the measured amplitude in frictional load for each cycle resulting in that cycle's average coefficient of static friction. All data sets represent 120 linear cycles. The data plotted in Fig. 8B indicates that the coefficient of static friction is higher in the 28 MPa (4,000 psi) hydrogen than in ambient air for the majority of the experiment. The mean μ_s values for the samples tested in hydrogen after 80 cycles was 1.46+/-0.22 while the air-tested mean μ_s values were 1.15+/-0.003.

Interestingly, there is also significantly more variation in the measured coefficient of friction in the hydrogen case than in either ambient air or in high pressure argon. The root cause for this observed behavior is still under investigation. Similar tests in high pressure argon shown in the appendix exhibit variation on the order of the ambient air results. Repeated calibration runs in high pressure hydrogen did not exhibit this high variance behavior indicating that it is likely not due to issues with motion of the sample sled in the hydrogen environment. One potential explanation of the variation is that chemical fillers in the NBR material are hydriding in the prescence of hydrogen and influencing the local mechanical properties of the

surface. Since the fillers are not necessarily evenly distributed throughout the sample, this could lead to larger variations in measured friction factors.

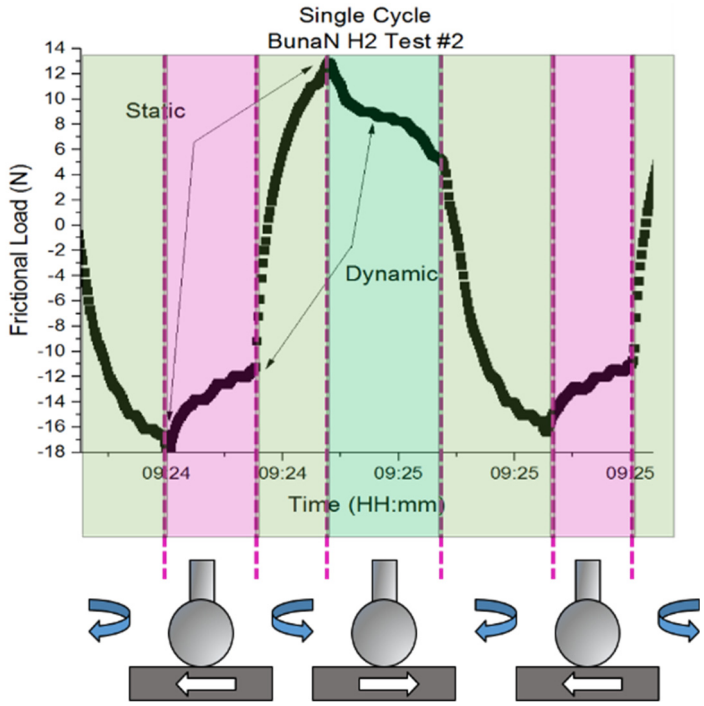

Figure 7. Characteristic frictional load curve for a single forward and reverse cycle of the sample stage overlayed with a schematic describing the forward (magenta), reverse (green) and transitional (yellow-green) areas of motion.

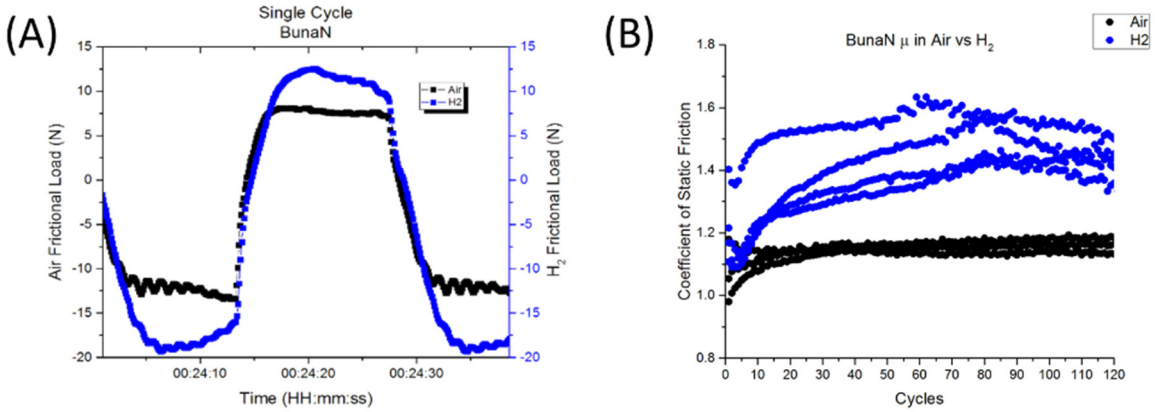

Figure 8. (A) Characteristic single cycle frictional force curve obtained for Buna N (NBR) in ambient air (black) overlayed with a characteristic single cycle frictional load curve obtained in hydrogen (blue). (B) Coefficients of static friction obtained in ambient air (black) and hydrogen (blue) for the same NBR sample.

11.1 In Situ Depth Measurements

In addition to coefficient of friction measurements, one typically measures the wear of the material. Our system has been set up to measure the differential depth of the ball into the polymer sample as a function of the cycling. Since it is possible that material is in some cases merely displaced by the motion of the ball

rather than physically eroded, this may not be a strict one-to-one correlation with ex situ wear depth measurements. Typically for polymers, one defines a wear factor, K as follows in Eq. 2.

$$X = K \text{ x } P \text{ x } V \text{ X } T$$

Equation 2. Wear depth in terms of: wear factor, K; normal pressure, P; velocity, V; and time, T.

Where X is the wear depth, K is the wear factor, P is the normal pressure, V is the velocity, and T is the time.[75] We then can define K* as follows in Eq. 3.

$$K^* = \frac{X}{P \text{ x } V \text{ x } T}$$

Equation 3. Surface damage and wear factor, K^*

The superscript * is used here to denote that some of the change in depth may be due to material displacement rather than removal of material, so we will more generally refer to K* as a surface damage and wear factor (SDWF) rather than strictly a wear factor (WF). We can then make ex situ comparisons and correlations with wear factors measured with optical profilometry. The wear factor is known to be highly dependent on P and V for polymers.[75] For a given environment though, the SDWF should be a constant.

11.2 In Situ Pressurization and Depressurization LVDT Measurements

During preparation of samples for wear testing, one can also monitor the load cell and LVDT during pressurization and depressurization which can measure changes in the sample dimension and can also be used as a check that the load cell is responding normally. As can be seen in Figure 9, the load decreases by approximately 9 N and then recovers by the same amount upon depressurization as expected. The LVDT shows that on average the sample thickness decreases by approximately 0.08 mm upon pressurization. This compression of the sample is not unexpected due to the pressure of the hydrogen gas. Upon decompression, the sample thickness (initially 3.175 mm) increases by approximately 1 mm. This slight over-recovery is due to trapped gas within the sample and in fact is readily visible as swelling upon removal of the sample. For comparison, the decrease in sample height for high pressure argon is similar, but the expansion is approximately 2 mm.

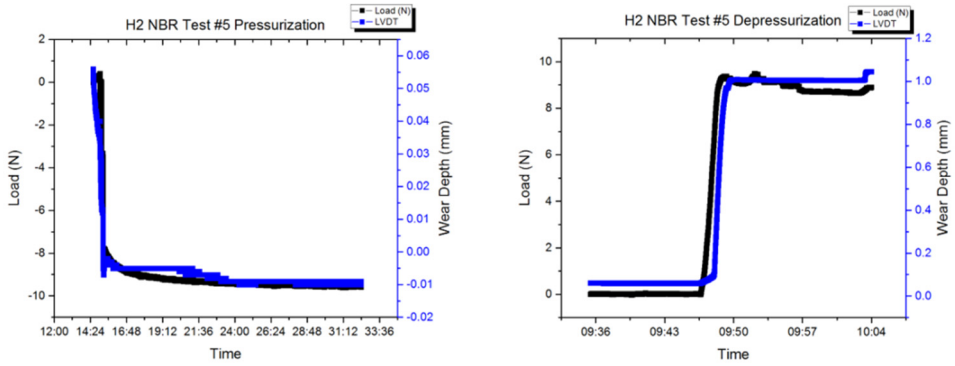

Figure 9. (LEFT) pressurization curves for the load cell and LVDT (depth). (RIGHT) similar curves for depressurization.

11.3 Ex Situ Hardness Testing and Swelling Measurements

In addition to in situ friction and wear measurement, one can also readily measure ex situ post measurement swelling and changes in hardness. While this can be done with the sample used for friction and wear measurements, it is preferable to use a separate sample that is not subject to any compression due to mounting. Swelling is measured by comparing dimensions before and after exposure to hydrogen gas and can be expressed as a percentage for a given pressure, temperature, and gas species. Note that since swelling is primarily due to trapped gas in the polymer, it will be heavily time dependent and most polymers will recover as gas diffuses out of the sample. In a similar manner, hardness can be measured before and after testing on a representative sample. Here again, the effect should recover with time as gas diffuses out of the sample. In the case of hydrogen, some of the hydrogen absorption is due to the formation of hydrides and may not recover at room temperature. It is important to measure both hardness and swelling as a function of time after exposure to form a better understanding of these effects.

11.4 Ex Situ Wear Track Analysis

Once the in situ experiments are complete, the samples are imaged with an optical microscope to investigate the wear track and to quantify depth and damage in the different environments. These images also provide a qualitative method for comparing the wear behavior. Representative images for experiments using NBR in 28 MPa (4,000 psi) hydrogen at 24 °C and ambient air at 23 °C and 44% relative humidity after 120 cycles are presented in Fig. 10A and 10B respectively. The left-hand images in Fig. 10 are black-and-white while the images on the right-hand side are false-colored height maps indicating surface depth where the green/blue areas are lower than the red/orange areas. Using ISO 6601 as a guide, is the images show evidence of more pitting, depressions, cracking and generated debris in the samples tested in hydrogen. These images seem to suggest that there is more damage to the samples tested in hydrogen than those tested in air.

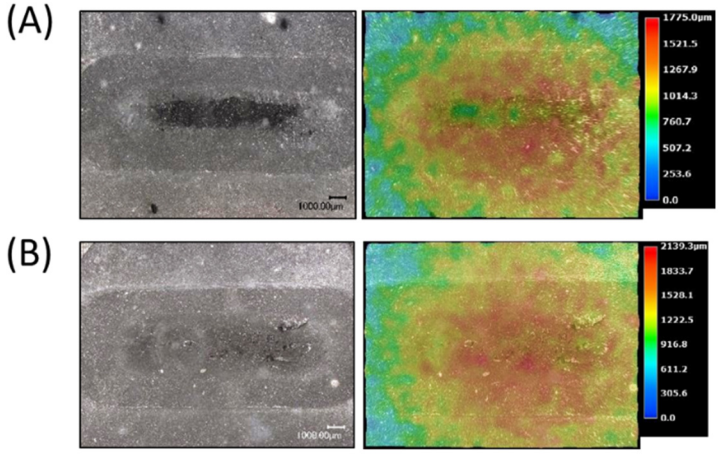

Figure 10. Gray-scale images and false-color wear depth maps of the wear tracks developed during the course of tribological testing of NBR samples in high-pressure hydrogen (A) and ambient air (B).

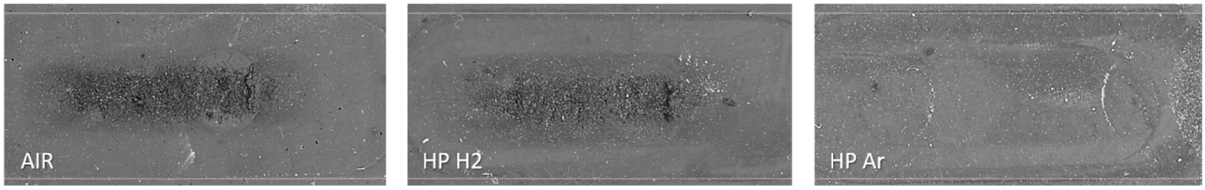

Figure 11. Gray-scale images of wear tracks at 120 cycles with the same loading in Air, high pressure (HP) H2, and HP Ar show qualitative differences in wear behavior

11.5 Temperature Effects

In addition to the above, a thorough understanding of the heating of the tribometer is critical as the heating from the various elements, most notably the motor, can potentially influence the sample temperature. To this end, we have done measurements in air of identical runs with IR thermal imaging and see that during the course of the run, the sample may increase in temperature as much as 8 °C. This is potentially problematic and future iterations of the system will incorporate both thermal measurement and control on the ball and the sample.

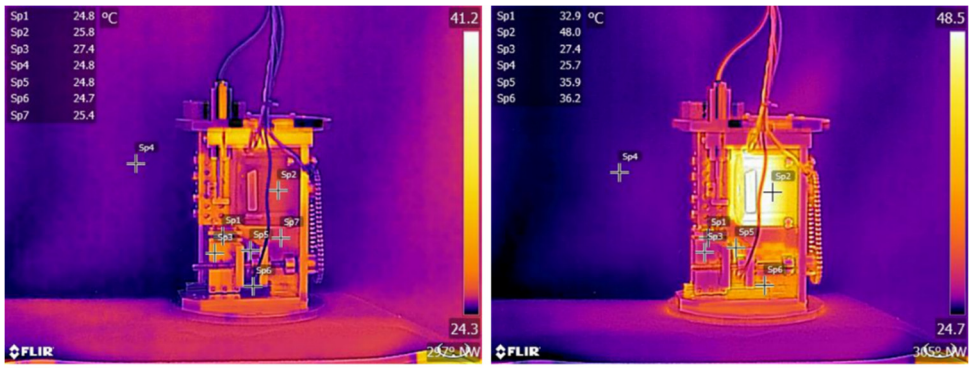

Before run Near end of run (~1 hr)

Figure 12. Thermal images of apparatus before experiment (LEFT) and near end of experiment (RIGHT).

12.0 Report

The following should be reported.

1. Velocity
2. Normal Force
3. Starting position
4. Humidity
5. Temperature
6. Pressure
7. Pressurization rate
8. Depressurization rate
9. Track length
10. LVDT measurement during pressurization, test, and depressurization
11. Load cell measurement during pressurization, test, and depressurization
12. Sample hardness before and after test
13. Sample dimensions before and after test
14. Monitor hardness and sample dimensions as a function of time after exposure

15. Optical profilometry of wear track
16. Duration of test
17. Duration of dwell time at test pressure
18. Oxygen level before hydrogen fill
19. Gas species
20. Calibration
21. Diameter of ball
22. Sample size
23. Sample thickness
24. Gas purity

13.0 Precision and Bias

13.1 Precision

For this system, the uncertainty in the data is dominated by variation from sample-to-sample. Due to the inhomogeneity of the fillers distributed in some materials and the wear characteristics of a given polymer in a certain gas, the precision of wear measurements for some materials may be higher than others. For example, materials with very little filler may produce more well-defined wear tracks than materials containing higher amounts of filler.

13.2 Repeatability and Reproducibility

As reported above, the sample-to-sample variation in the coefficient of friction data collected for ambient air and high-pressure argon and hydrogen environments was within 7%. This value is very similar in magnitude to the sample-to-sample variation measured for NBR using a commercial tribometer.

13.3 Bias

As in ASTM G133, there is no given reference material that can be used to determine the bias of the test methodologies contained within this report, therefore there is no basis to determine the bias in measurements gathered using these methodologies.

14.0 Discussion

As noted above, comparatively little is known about the effects of hydrogen on polymers as compared to hydrogen effects on metals and even ceramics. [3-5, 11, 12, 16, 18, 27, 43, 56, 59-61, 65, 67-73] There have been some limited investigations on tensile properties of HDPE[5] and the tribological properties of neat semi-crystalline polytetrafluoroethylene (PTFE)[12, 72, 73] and PTFE composites[68-71] in high pressure hydrogen. The process of hydrogen absorption in polymers is different from absorption in metals[62] due to a lack of disassociation in the polymer. Damaging effects may include bubble or void formation, surface blistering, dilation, changes in modulus and strength, and other changes associated with the absorption of a relatively high amount of hydrogen.[5] Additionally, since the saturation hydrogen concentrations in polymers is proportional to the exterior pressure it is thus expected that the damaging effects are more serious at higher pressures.[42, 49, 66] Some discussion of the effect of hydrogen on polymers is captured in reports by Sandia and Pacific Northwest National laboratories.[4, 74]

This preliminary test methodology represents one of the first of its kind in that it is designed particularly for polymers in high pressure hydrogen. To the authors' knowledge, there is only one standard available for polymer tribology, namely ISO 6601 which mainly describes damage mechanisms for the polymers.

While there are some hydrogen centric standards, namely, SAE J2579, J2601, the GTR, and the CSA/ANSI CHMC 1, none are focused on a materials level and polymers are not extensively covered. There is an effort underway with the development of the CSA CHMC 2 to develop a polymer centric standard for hydrogen compatibility of polymers, but this is still likely several years away from completion as of this writing.

15.0 Keywords

Keywords: hydrogen, tribology, reciprocating, friction, wear, polymer, elastomer

Appendix A

Supporting Data

A.1 Experimental

A.1.1 Sample Preparation

Samples are prepared from 25 mm wide and 3.175 mm thick strips of general purpose nitrile-butadiene rubber (NBR or Buna N) obtained from McMaster-Carr. The NBR strips were washed in water using dish soap to remove the talc powder from the surface. The washed strips were then dried in a 73 °C drying oven for 72 hours and stored in a dry box set to 25% relative humidity for another 72 hours. After washing and drying, the samples were cut into 22 mm diameter discs and the bottom surface was marked with an arrow to ensure that each sample was cut in the same orientation from a given NBR strip.

Experiments were carried out in both ambient air and high-pressure conditions with a custom-built linear reciprocating ball on flat sliding tribometer. A load controlled by the application of select dead weights is applied normal to the sample through a nearly spherical 6 mm diameter stainless steel shoulder tooling ball obtained from McMaster-Carr that is fixed in place and does not rotate. The ball is cleaned before each experiment using acetone. A total normal force of 12 N is provided by the combined weight of the copper dead weight and the brass static ball holder. During operation, the sample moves in a linear reciprocating fashion relative to the ball and the frictional load is measured with a coupled load cell. Samples are loaded onto the sample sled and secured in place using a frictional key-hole mounting plate and high precision compression springs. The sample is compressed by the mounting plate from 3.175 mm in height to 2.870 mm (12.9%) to ensure the sample stays in place during the experiment. The keyhole provides a large mounting area and prevents sample buckling and bowing that can occur due to sample expansion in hydrogen. The ball moves completely within the keyhole over a total wear track length of 14 mm.

A.1.1.1 Ambient Air testing

Experiments are performed in ambient air conditions to provide a basis of comparison for measurements performed in high pressure hydrogen and argon. The ambient air tests are performed inside a 15.5 L autoclave at room temperature that prevents any transient air currents from affecting the sample and frictional load measurement. Representative temperature and relative humidity measurements of the ambient environment inside the enclosure range from 21-26 °C and 33-54% respectively. Power and data electrical connections are then made and the tribometer is lowered onto two 0.8 mm thick copper O-rings for support and to offset the bottom plate of the instrument from the rounded bottom of the autoclave and then leveled. Once the tribometer is prepared, the stepper motor is run for 120 linear reciprocating cycles of the sample sled which takes approximately 60 minutes during which frictional load data is recorded. After the wear tests are complete, the samples are unloaded and then the wear track is imaged using a Keyence VHX-1000 microscope to qualitatively assess wear damage and measure track depth.

A.1.2 High Pressure Hydrogen and Argon Testing

The in situ high-pressure experiments are performed at room temperature inside the same autoclave used in ambient air testing. The tribometer is prepared for the experiments by mounting the samples and dead weights in the same manner as the ambient air tests. The autoclave cover containing all the electrical feedthroughs is then lowered onto a lens ring wrapped in Teflon tape and bolted onto the autoclave body. The bolts are torqued to 285 N*m to ensure a proper seal and prevent hydrogen leakage. 0.4 MPa (80 psi) argon is then flowed through the autoclave to displace any oxygen that may still be present. Once argon

has flowed for approximately one hour, the autoclave is then pressurized with hydrogen containing 0.5 ppm O_2 and H_2O in roughly 1.3 MPa (200 psi) steps to a final pressure of 28 MPa (4,000 psi). During the pressurization process an O_2 sensor is used to monitor the amount of O_2 present in the hydrogen flowing into the autoclave. The sample is soaked in hydrogen overnight to ensure complete saturation of the sample with hydrogen. Based on calculations using the literature values of the hydrogen diffusion rate in NBR, this should occur after approximately 2 hours for this sample thickness. By the next morning, the pressure in the autoclave drops to 26 MPa (3,800 psi) for hydrogen and 24 MPa (3,500 psi) for argon, due to a decrease in temperature after pressurization. The high pressure hydrogen experiment is then carried out in the same fashion as the ambient air experiments. After the experiment is complete, the autoclave is slowly depressurized at approximately 0.34 MPa/s (50 psi/s) and the tribometer is then removed. The samples are then unloaded and analyzed for wear damage.

A.1.3 Hardness Testing and Swelling Measurements

Samples of NBR, Viton and EPDM were placed on top of the tribometer during the high-pressure hydrogen and Argon testing, remaining in the autoclave during the overnight soak period and tribology experiment. These samples were used to measure the effects of these gas environments on the hardness and sample dimensions. These samples were prepared in a similar fashion as the tribology samples and cut using the same 22 mm die. Sample hardness was testing using a Shore "A-2" durometer compliant with ASTM D676 before exposure to high-pressure gas, directly afterwards and approximately seven days later. The diameter of these samples was measured using a digital caliper in a similar fashion: before exposure, directly after exposure, and seven days after exposure.

A.1.4 Wear Track Analysis (preliminary)

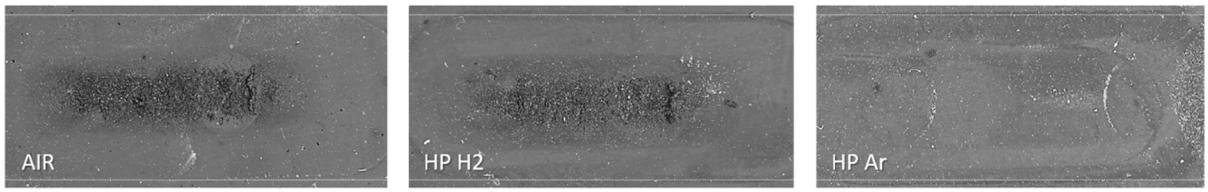

Figure 13. Gray-scale images of wear tracks at 120 cycles with the same loading in Air, high pressure (HP) H2, and HP Ar show qualitative differences in wear behavior.

A.2 Results

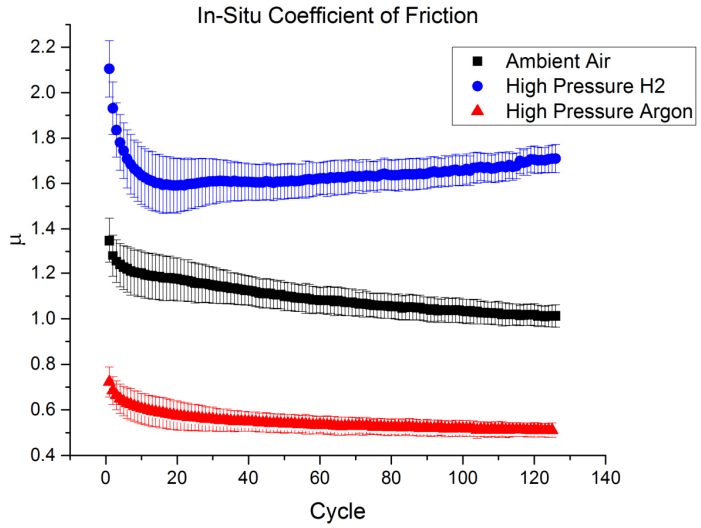

Figure 14. Mean and standard deviation of coefficient of static friction data determined using the described test methodology.

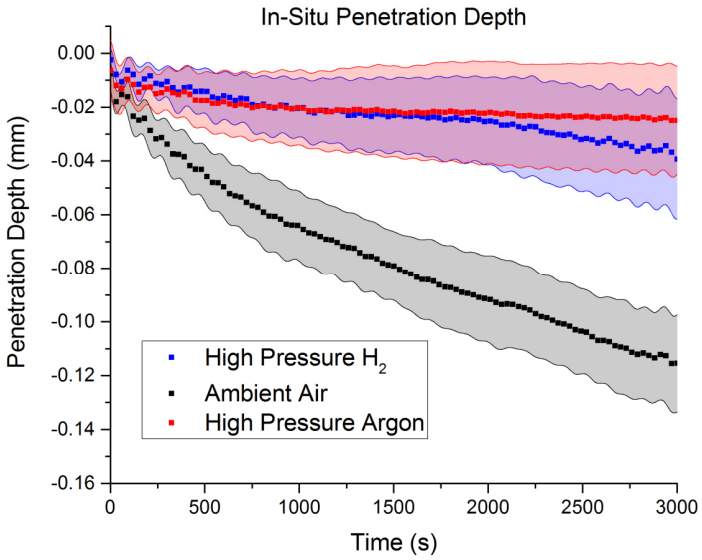

Figure 15: Mean and standard deviation of penetration depth data presented in Figure 14.

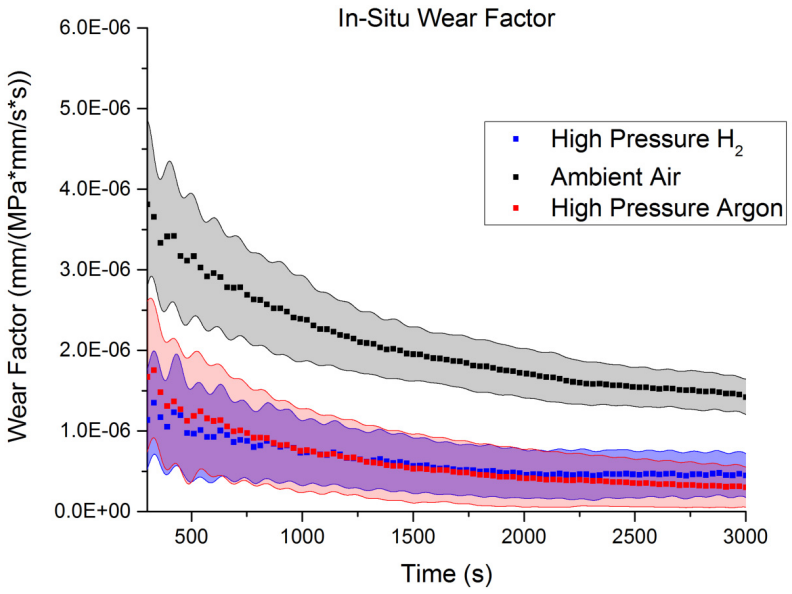

Figure 16. Surface damage and wear factor (K*) calculated for the LVDT data collected in Figure 15.

Table 1: Shore "A" hardness data for hydrogen and argon samples tested before, directly after, and one week after exposure.

H2 Shore "A" Hardness				
	NBR40	NBR50	EPDM	Viton
Rated	**40**	**50**	**60**	**75**
Pre-Exposure	46.5 +/- 0.3	51.8 +/- 0.4	63.1 +/- 0.2	74.8 +/- 0.2
Post- Exposure	40.5 +/- 0.4	41 +/- 0.6	53.3 +/- 0.6	70.2 +/- 0.8
1 week post-exposure	44.5 +/- 0.4	50.8 +/- 0.7	60.3 +/- 0.8	72.1 +/- 0.4
Ar Shore "A" Hardness				
	NBR40	NBR50	EPDM	Viton
Rated	**40**	**50**	**60**	**75**
Pre-Exposure	46.2 +/- 0.3	52.9 +/- 1.0	63.6 +/- 0.2	73 +/- 0.4
Post- Exposure	31.6 +/- 0.7	38.7 +/- 0.3	44.3 +/- 1.0	56.2 +/- 0.3
1 week post-exposure	38.6 +/- 0.4	51 +/- 0.4	53.3 +/- 0.6	70.5 +/- 0.4

Table 2: Measured dimensions of samples exposed to high pressure hydrogen and argon.

Dimensional Measurements (in millimeters)				
Hydrogen	NBR40	NBR50	EPDM	Viton
Pre-Exposure	21.86 +/- 0.1778		78.24 +/- 0.4623	
Post-Exposure	25.70 +/- 3.277		91.45 +/- 0.4623	
Change	117.57%		115.99%	
Argon	NBR40	NBR50	EPDM	Viton
Pre-Exposure	21.65 +/- 0.1372	21.56 +/- 0.1803	21.65 +/- 0.1270	21.49 +/- 0.1930
Post-Exposure	31.47 +/- 0.1524	23.05 +/- 0.2515	32.02 +/- 0.2794	23.23 +/- 0.1930
% Change	145.35%	106.92%	147.89%	108.11%
1 week later	22.40 +/- 0.1702	21.49 +/- 0.0737	22.29 +/- 0.1524	22.11 +/- 0.1270
% Change	103.45%	99.68%	102.97%	102.90%

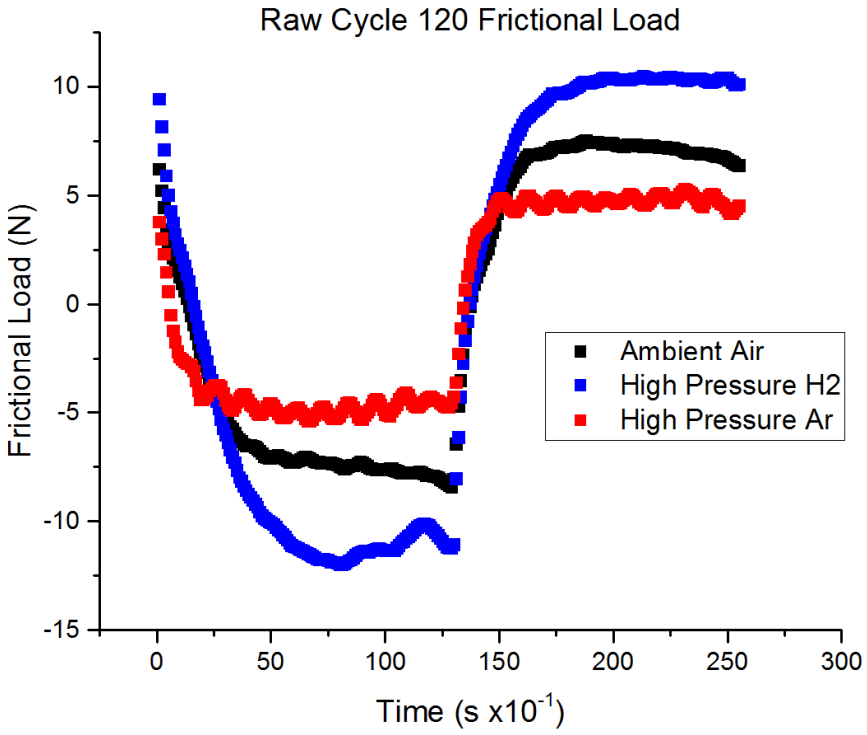

Figure 17: Mean-centered frictional load data of cycle #120 for high-pressure hydrogen, argon and ambient air.

Appendix B

References

1. Schlapbach, L., Technology: Hydrogen-fuelled vehicles. *Nature* **2009,** 460, (7257), 809-811.

2. Jones, R. H.; Thomas, G. J., *Materials for the hydrogen economy*. CRC Press: Boca Raton, 2008.

3. Barth, R. R.; Simmons, K. L.; SanMarchi, C., Polymers for Hydrogen Infrastructure and Vehicle Fuel Systems: Applications, Properties, and Gap Analysis. *SAND2013-8904* **2013**.

4. San Marchi, C.; Somerday, B. *Technical Reference on Hydrogen Compatibility of Materials, SAND2008-1163*; 2008.

5. Alvine, K. J.; Kafentzis, T. A.; Pitman, S. G.; Johnson, K. I.; Skorski, D.; Tucker, J. C.; Roosendaal, T. J.; Dahl, M. E., An in situ tensile test apparatus for polymers in high pressure hydrogen. *Review of Scientific Instruments* **2014,** 85, (10), -.

6. Welch, A.; Mumford, D.; Munshi, S.; Holbery, J.; Boyer, B.; Younkins, M.; Jung, H., Challenges in developing hydrogen direct injection technology for internal combustion engines. *SAE* **2008,** 2008-01-2379.

7. Waser, R., DIFFUSION OF HYDROGEN DEFECTS IN BATIO3 CERAMICS AND SRTIO3 SINGLE-CRYSTALS. *Berichte Der Bunsen-Gesellschaft-Physical Chemistry Chemical Physics* **1986,** 90, (12), 1223-1230.

8. Aggarwal, S.; Perusse, S. R.; Tipton, C. W.; Ramesh, R.; Drew, H. D.; Venkatesan, T.; Romero, D. B.; Podobedov, V. B.; Weber, A., Effect of hydrogen on Pb(Zr, Ti)O-3-based ferroelectric capacitors. *Applied Physics Letters* **1998,** 73, (14), 1973-1975.

9. Zhang, H.; Su, Y. J.; Qiao, L. J.; Chu, W. Y.; Wang, D.; Li, Y. X., The Effect of Hydrogen on the Fracture Properties of 0.8(Na1/2Bi1/2)TiO3-0.2(K1/2Bi1/2)TiO3 Ferroelectric Ceramics *Journal of Electronic Materials* **2008,** 37, (3), 368-372.

10. Park, C. H.; Chadi, D. J., Effect of Interstitial Hydrogen Impurities on Ferroelectric Polarization in PbTiO3. *Physical Review Letters* **2000,** 84, (20), 4717.

11. Sawae, Y.; Nakashima, K.; Doi, S.; Murakami, T.; Sugimura, J., Effects of High Pressure Hydrogen on Wear of PTFE and PTFE Composite. *ASME Conference Proceedings* **2009,** 2009, (48951), 233-235.

12. Y. Sawae, A. Y., K. Nakashima, T. Murakami, J. Sugimura, Effects of Hydrogen Atmosphere on Wear Behavior of PTFE Sliding Against Austenitic Stainless Steel. *Proceedings of ASME/STLE International Joint Tribology Conference* **2007**, 43-45.

13. Ren, X.; Chu, W.; Li, J.; Su, Y.; Qiao, L., The effects of inclusions and second phase particles on hydrogen-induced blistering in iron. *Materials Chemistry and Physics* **2008,** 107, (2–3), 231-235.

14. Han, J.-P.; Ma, T. P., *Electrode dependence of hydrogen-induced degradation in ferroelectric Pb(Zr,Ti)O3 and SrBi2Ta2O9 thin films*. AIP: 1997; Vol. 71, p 1267-1269.

15. Kushida-Abdelghafar, K.; Miki, H.; Torii, K.; Fujisaki, Y., Electrode-induced degradation of Pb(ZrxTi1-x)O-3 (PZT) polarization hysteresis characteristics in Pt/PZT/Pt ferroelectric thin-film capacitors. *Applied Physics Letters* **1996,** 69, (21), 3188-3190.

16. Sawae, Y.; Miyakoshi, E.; Doi, S.; Watanabe, H.; Kurono, Y.; Sugimura, J. In *Friction and Wear of Bronze Filled PTFE and Graphite Filled PTFE in 40 MPA Hydrogen Gas*, ASME/STLE 2011 International Joint Tribology Conference, 2011; American Society of Mechanical Engineers: 2011; pp 249-251.

17. Sugimura, J. In *Fundamental Studies on Tribology in Hydrogen*, International Hydrogen Conference (IHC 2012), 2014; ASME Press: 2014.

18. Boyer, S. A. E.; Gerland, M.; Castagnet, S., Gas environment effect on cavitation damage in stretched polyvinylidene fluoride. *Polymer Engineering & Science* **2014,** 54, (9), 2139-2146.

19. Alvine, K. J.; Shutthanandan, V.; Bennett, W. D.; Bonham, C. C.; Skorski, D.; Pitman, S. G.; Dahl, M. E.; Henager, C. H., High-pressure hydrogen materials compatibility of piezoelectric films. *Applied Physics Letters* **2010,** 97, (22), 221911.

20. Houde, D.; Lepine, Y.; Pepin, C.; Jandl, S.; Brebner, J. L., High-Resolution Infrared-Spectroscopy Of Hydrogen Impurities In Strontium-Titanate. *Physical Review B* **1987,** 35, (10), 4948-4953.

21. Yang, B.; Suh, C. W.; Lee, C. G.; Kang, E. Y.; Kang, Y. M.; Lee, S. S.; Hong, S. K.; Kang, N. S.; Yang, J. M., *Hydrogen barriers for SrBi2Ta2O9-based ferroelectric memories*. AIP: 2000; Vol. 77, p 1372-1374.

22. Alvine, K. J.; Vijayakumar, M.; Bowden, M. E.; Schemer-Kohrn, A. L.; Pitman, S. G., Hydrogen diffusion in lead zirconate titanate and barium titanate. *Journal of Applied Physics* **2012,** 112, (4), 043511.

23. Lu, G.; Kaxiras, E., Hydrogen embrittlement of aluminum: The crucial role of vacancies. *Physical Review Letters* **2005,** 94, (15), 155501.

24. Peng, X.; Su, Y. J.; Gao, K. W.; Qiao, L. J.; Chu, W. Y., Hydrogen fissure in PZT ferroelectric ceramic. *Materials Letters* **2004,** 58, (15), 2073-2075.

25. Nogami, M.; Shiiba, H.; Kleine, G. A.; Nakayama, M.; Hayakawa, T., Hydrogen Gas Permeation Through Al2O3-SiO2 Glasses Containing Metal Ions. *Journal of the American Ceramic Society* **2010,** 93, (11), 3752-3756.

26. Baikov, Y. M.; Shalkova, E. K., Hydrogen in perovskites. *Journal of Solid State Chemistry* **1992,** 97, (1), 224-227.

27. Castagnet, S.; Grandidier, J. C.; Comyn, M.; Benoit, G., Hydrogen influence on the tensile properties of mono and multi-layer polymers for gas distribution. *International Journal of Hydrogen Energy* **2010,** 35, (14), 7633-7640.

28. Alvine, K. J.; Tyagi, M.; Brown, C. M.; Udovic, T. J.; Jenkins, T.; Pitman, S. G., Hydrogen species motion in piezoelectrics: A quasi-elastic neutron scattering study. *Journal of Applied Physics* **2012,** 111, (5), 053505-7.

29. Eliaz, N.; Eliezer, D.; Olson, D. L., Hydrogen-assisted processing of materials. *Materials Science and Engineering A* **2000,** 289, (1-2), 41-53.

30. White, C. M.; Steeper, R. R.; Lutz, A. E., The hydrogen-fueled internal combustion engine: a technical review. *International Journal of Hydrogen Energy* **2006,** 31, (10), 1292-1305.

31. Wang, Y.; Chu, W.; Su, Y.; Qiao, L.; Gao, K., Hydrogen-induced cracking and its anisotropy of a PZT ferroelectric ceramics. *Science in China Series E: Technological Sciences* **2003,** 46, (3), 318-325.

32. Wang, Y.; Chu, W. Y.; Qiao, L. J.; Su, Y. J., Hydrogen-induced delayed fracture of PZT ceramics during dynamic charging under constant load. *Materials Science and Engineering B* **2003,** 98, (1), 1-5.

33. Shafiei, A.; Oprea, C.; Alfantazi, A.; Troczynski, T., In situ monitoring of the effects of hydrogen on Pb(Zr,Ti)O[sub 3] structure. *Journal of Applied Physics* **2011,** 109, (11), 114108.

34. Yamabe, J.; Nishimura, S., Influence of fillers on hydrogen penetration properties and blister fracture of rubber composites for O-ring exposed to high-pressure hydrogen gas. *International Journal of Hydrogen Energy* **2009,** 34, (4), 1977-1989.

35. Fukuda, K.; Sugimura, J., Influences of Trace Water in a Hydrogen Environment on the Tribological Properties of Pure Iron. *Tribology Online* **2013,** 8, (1), 22-27.

36. Sato, R.; Tomozawa, M., Interaction of water diffusion and hydrogen diffusion in silica glass at high temperatures. *Journal of Non-Crystalline Solids* **2004,** 343, (1-3), 26-32.

37. Zafar, S.; Kaushik, V.; Laberge, P.; Chu, P.; Jones, R. E.; Hance, R. L.; Zurcher, P.; White, B. E.; Taylor, D.; Melnick, B.; Gillespie, S., Investigation of hydrogen induced changes in SrBi2Ta2O9 ferroelectric films. *Journal of Applied Physics* **1997,** 82, (9), 4469-4474.

38. Lee, J. K.; Park, Y.; Chung, I., Investigation of hydrogen-induced degradation in Pb(ZrxTi1-x)O-3 thin film capacitors for the application of memory devices. *Journal of Applied Physics* **2002,** 92, (5), 2724-2728.

39. Shin, S.; Pi, U. H.; Kim, D. J.; Kang, B. S.; Noh, T. W.; Khim, Z. G., Investigation on hydrogen annealing effect for various ferroelectric films by electrostatic force microscope. *Applied Surface Science* **2002,** 188, (3-4), 411-415.

40. Castagnet, S.; Grandidier, J. C.; Comyn, M.; Benoît, G., Mechanical Testing of Polymers in Pressurized Hydrogen: Tension, Creep and Ductile Fracture. *Experimental Mechanics* **2012,** 52, (3), 229-239.

41. Jaravel, J.; Castagnet, S.; Grandidier, J.-C.; Benoît, G., On key parameters influencing cavitation damage upon fast decompression in a hydrogen saturated elastomer. *Polymer Testing* **2011,** 30, (8), 811-818.

42. Ahluwalia, R. K.; Hua, T. Q.; Peng, J. K., On-board and Off-board performance of hydrogen storage options for light-duty vehicles. *International Journal of Hydrogen Energy* **2012,** 37, (3), 2891-2910.

43. Kane, M. *Permeability, Solubility, and Interaction of Hydrogen in Polymers - An Assessment of Materials for Hydrogen Transport*; SRS: 2008.

44. Fuel Cell Technologies Office, D. E. In *Polymer and Composite Materials Used in Hydrogen Service: SAND2012-10860P*, Polymer and Composite Materiasl Meeting, Washington DC, 2012; Washington DC, 2012.

45. Theiler, G.; Gradt, T. In *Polymer composites for tribological applications in hydrogen environment*, Proceedings of the 2nd International Conference on Hydrogen Safety, 2007; 2007.

46. Lin, E. K.; Wu, W.-l.; Satija, S. K., Polymer Interdiffusion near an Attractive Solid Substrate. *Macromolecules* **1997,** 30, (23), 7224-7231.

47. Erck, R. A.; Fenske, G. R. In *Polymers and Coatings for Tribological Application in Hydrogen Environment*, International Hydrogen Conference (IHC 2012), 2014; ASME Press: 2014.

48. Hong, S. K.; Suh, C. W.; Lee, C. G.; Lee, S. W.; Kang, E. Y.; Kang, N. S.; Hwang, C. S.; Kwon, O. S., Protection of SrBi2Ta2O9 ferroelectric capacitors from hydrogen damage by optimized metallization for memory applications. *Applied Physics Letters* **2000,** 77, (1), 76-78.

49. Mori, D.; Hirose, K., Recent challenges of hydrogen storage technologies for fuel cell vehicles. *International Journal of Hydrogen Energy* **2009,** 34, (10), 4569-4574.

50. Yoon, S.-G.; Kingon, A. I., Recovery Characteristics of Hydrogen-Damaged (Pb, La)(Zr, Ti)O[sub 3] Capacitors with Pt and IrO[sub 2] Top Electrodes. *Journal of The Electrochemical Society* **2001,** 148, (7), F137-F139.

51. Deas Jr, T. M.; Hofer, H. H.; Dole, M., Solubility of hydrogen in polyethylene by a semimicro method. *Macromolecules* **1972,** 5, (2), 223-226.

52. Anyalebechi, P.; Talbot, D.; Granger, D., The solubility of hydrogen in solid binary aluminum-lithium alloys. *Metallurgical and Materials Transactions B* **1989,** 20, (4), 523-533.

53. Lee, H., The solubility of hydrogen in transition metals. *Metallurgical and Materials Transactions A* **1976,** 7, (3), 431-433.

54. Gradt, T.; Theiler, G., Tribological behaviour of solid lubricants in hydrogen environment. *Tribology Online* **2011,** 6, (2), 117-122.

55. Theiler, G.; Gradt, T., Tribological characteristics of polyimide composites in hydrogen environment. *Tribology International* **2015,** 92, 162-171.

56. Sawae, Y.; Fukuda, K.; Miyakoshi, E.; Doi, S.; Watanabe, H.; Nakashima, K.; Sugimura, J. In *Tribological Characterization of Polymeric Sealing Materials in High Pressure Hydrogen Gas*, STLE/ASME 2010 International Joint Tribology Conference, 2010; American Society of Mechanical Engineers: 2010; pp 251-253.

57. Fukuda, K.; Sawae, Y.; Miyakoshi, E.; Hashimoto, M.; Tanaka, H.; Watanabe, H.; Doi, S.; Sugimura, J. In *Tribological Properties of Austenitic Stainless Steel in Pressurized Hydrogen up to 40 MPa*, STLE/ASME 2010 International Joint Tribology Conference, 2010; American Society of Mechanical Engineers: 2010; pp 243-245.

58. Wu, M.; Huang, H. Y.; Chu, W. Y.; Guo, L. Q.; Qiao, L. J. E.; Xu, J. Y.; Zhang, T. Y., Tuning the Ferroelectric and Piezoelectric Properties of 0.91Pb(Zn1/3Nb2/3)O-3-0.09PbTiO(3) Single Crystals and

Lead Zirconate Titanate Ceramics by Doping Hydrogen. *Journal of Physical Chemistry C* **2010,** 114, (21), 9955-9960.

59. Sawae, Y.; Yamaguchi, A.; Nakashima, K.; Murakami, T.; Sugimura, J. In *Wear Behavior of Polymeric Sealing Material in Gaseous Hydrogen*, STLE/ASME 2008 International Joint Tribology Conference, 2008; American Society of Mechanical Engineers: 2008; pp 15-17.

60. Nakashima, K.; Morillo, C.; Kurono, Y.; Sawae, Y.; Sugimura, J. In *Wear Mechanisms of PTFE in Humidified Hydrogen Gas*, ASME/STLE 2011 International Joint Tribology Conference, 2011; American Society of Mechanical Engineers: 2011; pp 229-231.

61. Wisander, D. W.; Johnson, R. L. *Wear Rate and Friction Coefficient in Liquid Nitrogen and Hydrogen of Steel Sliding on Polymer Laminates (Various Fabrics and Polymers*; DTIC Document: 1968.

62. Fukai, Y. The Metal-Hydrogen System Basic Bulk Properties. http://dx.doi.org/10.1007/3-540-28883-X

63. Zhao, Z.; Carpenter, M., Annealing enhanced hydrogen absorption in nanocrystalline Pd⁄ Au sensing films. *Journal of Applied Physics* **2005,** 97, (12), 124301.

64. Ikarashi, N., Analytical transmission electron microscopy of hydrogen-induced degradation in ferroelectric Pb(Zr, Ti)O-3 on a Pt electrode. *Applied Physics Letters* **1998,** 73, (14), 1955-1957.

65. Yamabe, J.; Matsumoto, T.; Nishimura, S., Application of acoustic emission method to detection of internal fracture of sealing rubber material by high-pressure hydrogen decompression. *Polymer Testing* **2011,** 30, (1), 76-85.

66. Zheng, J.; Liu, X.; Xu, P.; Liu, P.; Zhao, Y.; Yang, J., Development of high pressure gaseous hydrogen storage technologies. *International Journal of Hydrogen Energy* **2012,** 37, (1), 1048-1057.

67. Sakano, Y.; Iwai, T.; Shoukaku, Y. In *Friction and Wear Properties of PTFE Composites Against 6061-T6 Aluminum Alloy Under Hydrogen Atmosphere*, ASME/STLE 2011 International Joint Tribology Conference, 2011; American Society of Mechanical Engineers: 2011; pp 397-399.

68. Yoshinori Sawae, K. F., Eiichi Miyakoshi, Shunichiro Doi, Hideki Watanabe, Kazuhiro Nakashima, Joich Sugimura, Tribological Characterization of Polymeric Sealing Materials in High Pressure Hydrogen Gas. *Proceedings of the STLE/ASME 2010 International Joint Tribology Conference* **2010**, 251-253.

69. Y. Sakano, T. I., Y. Shoukaku, Friction and Wear Properties of PTFE Composites Against 6061-T6 Aluminum Alloy Under Hydrogen Atmosphere. *Proceedings of the ASME/STLE 2011 International Joint Tribology Conference* **2011**, 397-399.

70. Yoshinori Sawae, E. M., Shunichiro Doi, Hideki Watanabe, Yoshie Kurono, Joichi Sugimura, Friction and Wear of Bronze Filled PTFE and Graphite Filled PTFE in 40 MPA Hydrogen Gas. *Proceedings of the ASME/STLE 2011 International Joint Tribology Conference* **2011**, 249-251.

71. Y. Sawae, K. N., S. Doi, T. Murakami, J. Sugimura, Effects of High Pressure Hydrogen on Wear of PTFE and PTFE Composite. *Proceedings of the ASME/STLE 2009 International Joint Tribology Conference* **2009**, 233-235.

72. Kazuhiro Nakashima, C. M., Yoshie Kurono, Yoshinori Sawae, Joichi Sugimura, Wear Mechanisms of PTFE in Humidified Hydrogen Gas. *Proceedings of the ASME/STLE 2011 International Joint Tribology Conference* **2011**, 229-231.

73. Y. Sawae, A. Y., K. Nakashima, T. Murakami, J. Sugimura, Wear Behavior of Polymeric Sealing Material in Gaseous Hydrogen. *Proceedings of STLE/ASME International Joint Tribology Conference* **2008**, 15-17.

74. Barth, R.; Simmons, K.; San Marchi, C., Polymers for Hydrogen Infrastructure and Vehicle Fuel Systems. *This report is available at* http://prod. *sandia. gov/techlib/access-control. cgi/2013/138904. pdf* **2013**.

75. McKeen, L. W., *Fatigue and Tribological Properties of Plastics and Elastomers*. 3rd ed.; William Andrew: Oxford, 2016.

Pacific Northwest
NATIONAL LABORATORY

Proudly Operated by **Battelle** *Since 1965*

U.S. DEPARTMENT OF
ENERGY

902 Battelle Boulevard
P.O. Box 999
Richland, WA 99352
1-888-375-PNNL (7665)

www.pnnl.gov